Localized Data Assimilation in the Ionosphere-Thermosphere Using a Sampled-Data Unscented Kalman Filter

I. S. Kim, D. J. Pawlowski, A. J. Ridley, D. S. Bernstein

Abstract— We apply the unscented Kalman filter (UKF) to data assimilation based on the vertical one-dimensional global ionosphere-thermosphere model, which models the highly coupled, strongly nonlinear Earth's upper atmosphere. To reduce the computational complexity of UKF, we introduce a localized, sampled-data update scheme with frozen-intersample error covariance, and examine its performance through numerical simulation.

I. INTRODUCTION

For nonlinear estimation and data assimilation, the terrestrial weather forecasting community has largely adopted the ensemble Kalman filter (EnKF) [1–6]. This technique retains the data injection form of the Kalman filter but does not propagate the error covariance in the classical manner. Instead, EnKF propagates an ensemble of systems under random forcing and initial states to estimate the error covariance. This technique is applicable in principle to highly nonlinear systems. Although the size of the ensemble affects the accuracy of the estimates, there are no theoretical guidelines for determining the size of the ensemble.

For applications involving nonlinear and non-Gaussian systems [7], particle filters are used. A particle filter obtains estimates through Monte Carlo simulation at each step using an assumed probability density function and resampling technique [8]. Although particle filters can estimate the state of a nonlinear system with a non-Gaussian probability density, there is no definitive guideline for determining the number of sample points for achieving good accuracy.

In contrast with the ensemble Kalman filter and particle filters, the unscented Kalman filter (UKF) uses a deterministic number of ensemble members (specifically, $2n + 1$ ensemble members, where n is the number of states of the system) to estimate the error covariance and obtain the data-injection gain [9, 10]. The fundamental component of UKF is the unscented transformation, which uses a minimal set of specially chosen weighted points to parameterize the mean and covariance of the state probability distribution. These sample points, which capture the mean and covariance of a Gaussian random variable, are propagated through the model to capture the posterior mean and covariance to second order for smooth but arbitrary nonlinearities. Furthermore, UKF treats the model and its software implementation as a black box, which eliminates the need to construct a Jacobian as required by the extended Kalman filter (XKF) [11].

In view of these advantages, the goal of the present paper is to apply UKF to data assimilation for space weather applications. In particular, we focus on the Earth's atmosphere between 100 km and 1000 km altitude, a region known as the ionosphere-thermosphere. For this objective we use the parallel global ionosphere-thermosphere model (GITM) code as the basis of data assimilation. Using UKF, we eliminate the need for either the Jacobian required by XKF or a dynamics factorization required by the state-dependent Riccati equation (SDRE) filter [12]. In addition, for flow problems, UKF is significantly more accurate than XKF under highly nonlinear conditions [11].

For large-scale systems, however, the $2n + 1$ ensemble size of UKF presents a significant computational burden. For example, in vertical (altitude-only) 1D GITM, with $n = 700$, the total number of states in the UKF ensemble for GITM can reach 900,000, while, for the 3D case with $5°$ resolution in longitude and latitude, with $n = 1,814,400$, the total number of states exceeds 10^{13} (10 trillion). The resulting computational requirement necessitates localized UKF, wherein data injection is confined to a specified region, with coupling to data-free simulation in the exterior region [13, 14]. With this approach, data assimilation based on 3D GITM is feasible through parallel implementation on a multiprocessor cluster.

Data for GITM are provided by ground-based or space-based sensors. Since measurements are not available at every integration time step, we perform the unscented transformation to update the covariance and state only when measurement data are available. Between measurement update times, GITM runs in data-free simulation mode. Another relevant issue in data assimilation based on GITM is that data assimilation performance depends on the accuracy of the disturbance and measurement noise covariances. Due to the high nonlinearity of GITM, UKF is sensitive to the disturbance covariance and may become unstable or yield poor performance. Although the measurement noise covariance is known, a disturbance covariance must be constructed to capture the effect of external drivers. For the case of solar irradiation, we approximate the disturbance covariance by means of a Monte Carlo method. Alternative techniques are discussed in [15]

II. Sampled-Data UKF

Consider the discrete-time nonlinear system

$$x_{k+1} = f(x_k, u_k, k) + w_k \qquad (2.1)$$

and measurements

$$y_k = h(x_k, k) + v_k, \qquad (2.2)$$

where $x_k \in \mathbb{R}^n$, $u_k \in \mathbb{R}^m$, and $y_k \in \mathbb{R}^p$. The input u_k and output y_k are assumed to be measured, and $w_k \in \mathbb{R}^n$ and $v_k \in \mathbb{R}^p$ are uncorrelated zero-mean white noise processes with covariances Q_k and R_k, respectively. We assume that R_k is positive definite. The inputs u_k and w_k represent known and unknown physics drivers, respectively.

The starting point for UKF is a collection of state estimates or sample points that capture the initial probability distribution of the state. The unscented transformation is used to construct these sample points with a specified mean and variance.

To define this procedure, let $\bar{x} \in \mathbb{R}^n$, let $\bar{P} \in \mathbb{R}^{n \times n}$ be positive semidefinite, and let $\lambda > 0$. The unscented transformation provides $2n + 1$ sample points $X_i \in \mathbb{R}^n$ and corresponding weights $\gamma_{s,i}$ and $\gamma_{P,i}$ so that $\bar{x}$ and $\bar{P}$ are the weighted mean and weighted variance of the sample points, respectively. The unscented transformation

$$X = \Psi(\bar{x}, \bar{P}, \lambda) \in \mathbb{R}^{n \times (2n+1)} \qquad (2.3)$$

of $\bar{x}$ with covariance $\bar{P}$ is defined by

$$X_i = \begin{cases} \bar{x}, & \text{if } i = 0, \\ \bar{x} + \sqrt{\lambda}\tilde{P}_i, & \text{if } i = 1, \dots, n, \\ \bar{x} - \sqrt{\lambda}\tilde{P}_{i-n}, & \text{if } i = n+1, \dots, 2n, \end{cases} \qquad (2.4)$$

where $\tilde{P}_i$ is the ith column of $\tilde{P} \in \mathbb{R}^{n \times n}$, which satisfies $\tilde{P}^{\mathrm{T}}\tilde{P} = \bar{P}$, and X_i is the ith column of X. The parameter $\lambda > 0$ determines the spread of the sample points around $\bar{x}$ but can otherwise be chosen arbitrarily. Note that

$$\sum_{i=0}^{2n} \gamma_{s,i} X_i = \bar{x}, \quad \sum_{i=0}^{2n} \gamma_{P,i}(X_i - \bar{x})(X_i - \bar{x})^{\mathrm{T}} = \bar{P}, \quad (2.5)$$

where the weights $\gamma_{s,i}$ and $\gamma_{P,i}$ are defined by

$$\gamma_{s,0} \triangleq 1 - \frac{n}{\lambda}, \quad \gamma_{P,0} \triangleq 1 - \frac{n}{\lambda} + \left(1 - \frac{\lambda}{n} + \beta\right), \quad (2.6)$$

$$\gamma_{s,i} = \gamma_{P,i} \triangleq \frac{1}{2\lambda}, \quad i = 1, \dots, 2n. \qquad (2.7)$$

The parameter $\beta \geq 0$ can be chosen arbitrarily; it is customary to set $\beta = 2$.

UKF uses the unscented transformation to update the state estimate by simulating $2n + 1$ copies of the model with the initial conditions $X_0, \dots, X_{2n}$, and by using the propagated states to approximate the mean and covariance of the state error. We assume that an initial estimate x_0^{f} of the state x_0 is given along with an initial error covariance $P_0^{\mathrm{f}} \in \mathbb{R}^{n \times n}$.

For data assimilation based on GITM, we consider simulated data that are representative of an incoherent scatter radar (ISR). The ISR data update rate is typically much slower than the GITM integration time step. For the present study, we implement UKF for GITM with state and error-covariance measurement updates occurring every 60 seconds,

whereas the integration time step for the GITM advection equations is 1 second.

Between measurement updates, the standard approach is to propagate the error-covariance in open loop. However, since the major dynamics of GITM are slow compared to the measurement update rate, we freeze the error covariance between measurement updates. A similar technique is used in [16, 17].

The sampled-data UKF with data available every N steps and with frozen intersample error covariance is illustrated in Figure 1. We assume that measurements are available at the sample instants $k = N, 2N, 3N, \dots$.

The UKF data assimilation step for $k = iN$ given $x_k^{\mathrm{f}}, P_k^{\mathrm{f}}, \lambda, y_k$, and R_k is given by

$$X_k^{\mathrm{f}} \triangleq \Psi(x_k^{\mathrm{f}}, P_k^{\mathrm{f}}, \lambda), \qquad (2.8)$$

$$Y_{i,k}^{\mathrm{f}} \triangleq h(X_{i,k}^{\mathrm{f}}, k), \qquad (2.9)$$

$$y_k^{\mathrm{f}} \triangleq \sum_{i=0}^{2n} \gamma_{s,i} Y_{i,k}^{\mathrm{f}}, \qquad (2.10)$$

$$P_{\mathrm{xy},k} \triangleq \sum_{i=0}^{2n} \gamma_{P,i}(X_{i,k}^{\mathrm{f}} - x_k^{\mathrm{f}})(Y_{i,k}^{\mathrm{f}} - y_k^{\mathrm{f}})^{\mathrm{T}}, \qquad (2.11)$$

$$P_{\mathrm{yy},k} \triangleq \sum_{i=0}^{2n} \gamma_{P,i}(Y_{i,k}^{\mathrm{f}} - y_k^{\mathrm{f}})(Y_{i,k}^{\mathrm{f}} - y_k^{\mathrm{f}})^{\mathrm{T}} + R_k, \quad (2.12)$$

$$K_k \triangleq P_{\mathrm{xy},k} P_{\mathrm{yy},k}^{-1}, \qquad (2.13)$$

$$x_k^{\mathrm{da}} = x_k^{\mathrm{f}} + K_k(y_k - y_k^{\mathrm{f}}), \qquad (2.14)$$

$$P_k^{\mathrm{da}} = P_k^{\mathrm{f}} - K_k P_{\mathrm{yy},k} K_k^{\mathrm{T}}. \qquad (2.15)$$

The UKF forecast step for $k = iN$ given $x_k^{\mathrm{da}}, P_k^{\mathrm{da}}, \lambda, u_k$, and Q_k is given by

$$X_k^{\mathrm{da}} \triangleq \Psi(x_k^{\mathrm{da}}, P_k^{\mathrm{da}}, \lambda), \qquad (2.16)$$

$$\tilde{X}_{i,k+1}^{\mathrm{f}} = f(X_{i,k}^{\mathrm{da}}, u_k, k), \qquad (2.17)$$

$$x_{k+1}^{\mathrm{f}} \triangleq \sum_{i=0}^{2n} \gamma_{s,i} \tilde{X}_{i,k+1}^{\mathrm{f}}, \qquad (2.18)$$

$$P_{k+1}^{\mathrm{f}} = \sum_{i=0}^{2n} \gamma_{P,i}(\tilde{X}_{i,k+1}^{\mathrm{f}} - x_{k+1}^{\mathrm{f}})(\tilde{X}_{i,k+1}^{\mathrm{f}} x_{k+1}^{\mathrm{f}})^{\mathrm{T}} + Q_k. \qquad (2.19)$$

The UKF forecast step for $k = iN+1, \dots, (i+1)N-1$ given x_k^{f}, u_k, and P_k^{f} is given by

$$x_{k+1}^{\mathrm{f}} = f(x_k^{\mathrm{f}}, u_k, k), \qquad (2.20)$$

$$P_{k+1}^{\mathrm{f}} = P_k^{\mathrm{f}} \text{ (frozen)}. \qquad (2.21)$$

III. Localized UKF

UKF estimates all states through data injection. In particular, for a system with n states, UKF requires $2n + 1$ simulation model updates, which are used to update the $n \times n$ covariance. If n is large, as in the case of GITM, then the computational burden of implementing UKF is enormous. We address this problem by performing UKF updates of both the states and the error covariance locally while treating the subsystem coupling terms as known inputs. The benefit
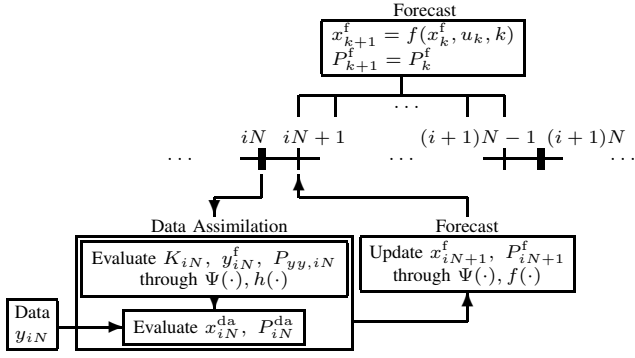
Fig. 1. Timing diagram of sampled-data UKF with frozen intersample error covariance.

of data assimilation thus reaches the entire system through coupling between the localized and exterior regions.

Assume that the state $x_k \in \mathbb{R}^n$ has the components

$$x_k = \begin{bmatrix} x_{\mathrm{L},k} \\ x_{\mathrm{E},k} \end{bmatrix}, \tag{3.1}$$

where $x_{\mathrm{L},k} \in \mathbb{R}^{n_{\mathrm{L}}}$ and $x_{\mathrm{E},k} \in \mathbb{R}^{n_{\mathrm{E}}}$ denote the states of the localized and exterior regions, respectively, and $n_{\mathrm{L}} + n_{\mathrm{E}} = n$. We, assume that the measurements depend entirely on the state $x_{\mathrm{L},k}$ so that y_k can be expressed as

$$y_k = h(x_{\mathrm{L},k}, k) + v_k. \tag{3.2}$$

Finally, partition Q_k and P_k as

$$Q_k = \begin{bmatrix} Q_{\mathrm{L},k} & Q_{\mathrm{LE},k} \\ Q_{\mathrm{LE},k}^{\mathrm{T}} & Q_{\mathrm{E},k} \end{bmatrix}, P_k = \begin{bmatrix} P_{\mathrm{L},k} & P_{\mathrm{LE},k} \\ (P_{\mathrm{LE},k})^{\mathrm{T}} & P_{\mathrm{E},k} \end{bmatrix}. \tag{3.3}$$

The objective is to directly inject the measurement data y_k into only the states corresponding to the estimate of $x_{\mathrm{L},k}$ by using a reduced-order error covariance.

In the data assimilation step of UKF, we inject data into the $x_{\mathrm{L},k}$ subsystem and update $P_{\mathrm{L},k}^{\mathrm{f}}$ as if only the $x_{\mathrm{L},k}$ subsystem were present. However, in the forecast step (2.17)-(2.19), we update the full state vector $X_{i,k} \in \mathbb{R}^n$ through the dynamics $f(\cdot)$ in (2.17) but with the number of ensembles reduced from $2n + 1$ to $2n_{\mathrm{L}} + 1$ since the ensembles are determined from $P_{\mathrm{L},k}^{\mathrm{da}} \in \mathbb{R}^{n_{\mathrm{L}} \times n_{\mathrm{L}}}$. This technique is the localized unscented Kalman filter (LUKF) [13, 14].

LUKF data assimilation step for $k = N, 2N, 3N, \dots$ is given by

$$X_{\mathrm{L},k}^{\mathrm{f}} \triangleq \Psi(x_{\mathrm{L},k}^{\mathrm{f}}, P_{\mathrm{L},k}^{\mathrm{f}}, \lambda), \tag{3.4}$$

$$Y_{i,k}^{\mathrm{f}} \triangleq h(X_{\mathrm{L},i,k}^{\mathrm{f}}, k), \tag{3.5}$$

$$y_k^{\mathrm{f}} \triangleq \sum_{i=0}^{2n_{\mathrm{L}}} \gamma_{\mathrm{s},i} Y_{i,k}^{\mathrm{f}}, \tag{3.6}$$

$$P_{\mathrm{xLy},k} \triangleq \sum_{i=0}^{2n_{\mathrm{L}}} \gamma_{\mathrm{P},i} (X_{\mathrm{L},i,k}^{\mathrm{f}} - x_{\mathrm{L},k}^{\mathrm{f}})(Y_{i,k}^{\mathrm{f}} - y_k^{\mathrm{f}})^{\mathrm{T}}, \tag{3.7}$$

$$P_{\mathrm{yy},k} \triangleq \sum_{i=0}^{2n_{\mathrm{L}}} \gamma_{\mathrm{P},i} (Y_{i,k}^{\mathrm{f}} - y_k^{\mathrm{f}})(Y_{i,k}^{\mathrm{f}} - y_k^{\mathrm{f}})^{\mathrm{T}} + R_k, \tag{3.8}$$

$$K_{\mathrm{L},k} \triangleq P_{\mathrm{xLy},k} P_{\mathrm{yy},k}^{-1}, \tag{3.9}$$

$$x_{\mathrm{L},k}^{\mathrm{da}} = x_{\mathrm{L},k}^{\mathrm{f}} + K_{\mathrm{L},k}(y_k - y_k^{\mathrm{f}}), \tag{3.10}$$

$$x_{\mathrm{E},k}^{\mathrm{da}} = x_{\mathrm{E},k}^{\mathrm{f}} \tag{3.11}$$

$$P_{\mathrm{L},k}^{\mathrm{da}} = P_{\mathrm{L},k}^{\mathrm{f}} - K_{\mathrm{L},k} P_{\mathrm{yy},k} K_{\mathrm{L},k}^{\mathrm{T}}, \tag{3.12}$$

where, for $i = 0, \dots, 2n_{\mathrm{L}}$, $X_{\mathrm{L},i,k}^{\mathrm{f}} \in \mathbb{R}^{n_{\mathrm{L}}}$ is the $(i+1)$th column of $X_{\mathrm{L},k}^{\mathrm{f}}$. Note that only $2n_{\mathrm{L}} + 1$ ensembles are used rather than $2n + 1$ ensembles as in UKF, while (3.10)-(3.11) indicate that measurement data are injected directly into only the estimates of the state $x_{\mathrm{L},k}$ corresponding to the localized region.

The LUKF forecast step is given by

$$X_{\mathrm{L},k}^{\mathrm{da}} \triangleq \Psi(x_{\mathrm{L},k}^{\mathrm{da}}, P_{\mathrm{L},k}^{\mathrm{da}}, \lambda), \tag{3.13}$$

$$\tilde{X}_{i,k+1}^{\mathrm{f}} = f(X_{i,k}^{\mathrm{da}}, u_k, k), \tag{3.14}$$

$$x_{k+1}^{\mathrm{f}} \triangleq \sum_{i=0}^{2n_{\mathrm{L}}} \gamma_{\mathrm{s},i} \tilde{X}_{i,k+1}^{\mathrm{f}}, \tag{3.15}$$

$$P_{\mathrm{L},k+1}^{\mathrm{f}} = \sum_{i=0}^{2n_{\mathrm{L}}} \gamma_{\mathrm{P},i} (\tilde{X}_{\mathrm{L},i,k+1}^{\mathrm{f}} - x_{\mathrm{L},k+1}^{\mathrm{f}})(\tilde{X}_{\mathrm{L},i,k+1}^{\mathrm{f}} - x_{\mathrm{L},k+1}^{\mathrm{f}})^{\mathrm{T}}$$
$$+ Q_{\mathrm{L},k}. \tag{3.16}$$

where, for all $i = 0, \dots, 2n_{\mathrm{L}}$, $X_{i,k}^{\mathrm{da}} \in \mathbb{R}^n$, $\tilde{X}_{i,k+1}^{\mathrm{f}} \in \mathbb{R}^n$ have the form

$$X_{i,k}^{\mathrm{da}} \triangleq \begin{bmatrix} X_{\mathrm{L},i,k}^{\mathrm{da}} \\ x_{\mathrm{E},k}^{\mathrm{da}} \end{bmatrix}, \quad \tilde{X}_{i,k+1}^{\mathrm{f}} = \begin{bmatrix} \tilde{X}_{\mathrm{L},i,k+1}^{\mathrm{f}} \\ \tilde{X}_{\mathrm{E},i,k+1}^{\mathrm{f}} \end{bmatrix}, \quad (3.17)$$

where $X_{\mathrm{L},i,k}^{\mathrm{da}} \in \mathbb{R}^{n_{\mathrm{L}}}$ is the $(i+1)$th column of $X_{\mathrm{L},k}^{\mathrm{da}}$, and $\tilde{X}_{i,k+1}^{\mathrm{f}}$ has components $\tilde{X}_{\mathrm{L},i,k+1}^{\mathrm{f}} \in \mathbb{R}^{n_{\mathrm{L}}}$ and $\tilde{X}_{\mathrm{E},i,k+1}^{\mathrm{f}} \in \mathbb{R}^{n_{\mathrm{E}}}$. Notice that the estimate $x_{\mathrm{E},k}^{\mathrm{da}}$ of the state $x_{\mathrm{E},k}$ in all of the ensembles of LUKF in (3.17) is the same, whereas the estimate $X_{\mathrm{L},i,k}^{\mathrm{da}}$ of the state $x_{\mathrm{L},k}$ is different in each ensemble.

Although (3.11) implies that data are not directly injected into the state estimates corresponding to $x_{\mathrm{E},k}$, it follows from $X_{\mathrm{L},i,k}^{\mathrm{da}}$ in (3.17), (3.13), and (3.15) that the measurement data affect the estimates of the state $x_{\mathrm{E},k}$ through the dynamic coupling between $x_{\mathrm{L},k}$ and $x_{\mathrm{E},k}$. Since LUKF involves $2n_{\mathrm{L}} + 1$ model updates, the number of states involved is of the order $(2n_{\mathrm{L}} + 1)n$. Hence, when $n_{\mathrm{L}} \ll n$, LUKF is computationally less demanding than UKF.

IV. GITM MODEL AND INCOHERENT SCATTER RADAR MEASUREMENTS

The GITM is a fully parallel three-dimensional finite-volume model that simulates the coupled ionosphere-thermosphere system over the entire surface of the Earth in spherical coordinates. GITM for data assimilation is based on 14 state variables per cell, namely, the number densities of the neutral species O, O_2, N_2, N, the vertical velocities of each neutral species, the eastward and northward bulk neutral velocities u_ϕ, u_θ, respectively, the normalized neutral mean temperature $\mathcal{T}_n$, and the number densities of the ions O^+, O_2^+, and NO^+. Here, number density denotes the number of neutral molecules or ions per cubic meter. These state variables, which are updated by solving the equations of

continuity, momentum, and energy, are used to compute the number density of electrons N_e, the ion velocity $\mathbf{v}_{ion}$, and the ion temperature T_{ion}, which correspond to the part of incoherent scatter radar (ISR) measurement data. For a detailed description of the physics, dynamics, and numerical schemes, see [18].

While ISRs provide several data products [19], we consider the number density N_e of electron, the line-of-sight component of ion velocity $\mathbf{v}_{ion}$, and the ion temperature T_{ion}. All ions are assumed to move in same velocity $\mathbf{v}_{ion}$, while T_{ion} is the average value over the ion species. For 1D GITM, we assume that the radar is pointed vertically to measure the vertical component of ion velocity.

V. APPROXIMATING THE PROCESS NOISE COVARIANCE Q

The disturbance covariance Q, which determines the range of UKF perturbations, is a critical parameter for strongly nonlinear systems such as GITM. An inappropriate value of Q yields poor data assimilation performance including instability. Filter performance can be improved by taking Q to be proportional to the error covariance, a technique known as covariance inflation [20–22].

For GITM, we approximate Q based on the measurement update time step, which is much longer than the GITM integration time step. Basically, we assume that error-covariance propagation is dominated by the disturbance rather than the system dynamics during the measurement-update time interval, which implies that the error-covariance can be frozen between measurement updates.

We estimate Q based on the solar EUV irradiation $F_{10.7}$, which is one of several inputs to GITM. $F_{10.7}$ is a main GITM driver during calm periods, that is, when there are few geomagnetic storms. Since $F_{10.7}$ is largely unknown in the sense that only its daily average is known [23, 24], its variation is appropriately represented by w_k. Consequently, the process noise or disturbance input of GITM is assumed to come from the random variation of $F_{10.7}$.

A. Estimating the Covariance Q

At time step k, consider GITM with mean input $\bar{\mu}_k$, which represents mean value of $F_{10.7}$. The resulting state $\bar{x}_k$ propagates according to

$$\bar{x}_{k+N} = f^{(N)}(\bar{x}_k, \bar{\mu}_k), \tag{5.1}$$

where N is the number of steps in a sample period and $f^{(N)}(\cdot)$ is the mapping from time k to $k + N$.

Now consider GITM with inputs $\mu_{k,i} = \bar{\mu}_k + \Delta\mu_{k,i}$, $i = 1, \ldots, m$, where m is number of samples for Monte Carlo simulation, $\mu_{k,i}$ is $F_{10.7}$, $\bar{\mu}_k$ is the mean $F_{10.7}$, and $\Delta\mu_{k,i}$ is the deviation from the mean. The mean of $\Delta\mu_{k,i}$ is zero, and the corresponding standard deviation is chosen to be 3 times larger than the standard deviation of the daily $F_{10.7}$ variations. Hence

$$x_{k+N,i} = f^{(N)}(\bar{x}_k, \bar{\mu}_k + \Delta\mu_{k,i}) \tag{5.2}$$

$$\approx f^{(N)}(\bar{x}_k, \bar{\mu}_k) + \Delta\mu_{k,i}\eta_k, \tag{5.3}$$

where $\eta_k \triangleq \frac{\partial f^{(N)}}{\partial \mu_k}(\bar{x}_k, \bar{\mu}_k) \in \mathbb{R}^n$. In (5.3), the term $\Delta\mu_{k,i}\eta_k$ serves as the disturbance input. Using (5.1) and (5.3), we obtain

$$\Delta\mu_{k,i}\eta_k \approx x_{k+N,i} - f^{(N)}(\bar{x}_k, \bar{\mu}_k) \tag{5.4}$$

$$= x_{k+N,i} - \bar{x}_{k+N}. \tag{5.5}$$

Then, the process noise covariance $\tilde{Q}_k$ can be approximated as

$$\tilde{Q}_k \approx \frac{1}{m}\sum_{i=1}^{m}(\eta_k\Delta\mu_{k,i})(\eta_k\Delta\mu_{k,i})^{\mathrm{T}}. \tag{5.6}$$

To obtain a constant value of Q, we take Q to be the diagonal part of $\tilde{Q}_k$, where k is chosen such that $\operatorname{tr}\tilde{Q}_k$ achieves its maximum value over the simulation interval.

VI. OBSERVABILITY OF GITM FOR DATA ASSIMILATION

We assess the observability of GITM by changing the measurement locations and quantities used in data assimilation performed by UKF. We can thus select measurement locations and quantities to optimize estimation accuracy. For this study, we use a 1D vertical GITM model with 50 grid cells covering 100 km to 750 km in altitude at the location of Millstone Hill, MA, USA, where the Haystack Observatory is located [http://www.haystack.mit.edu/].

A. Effect of Measurement Locations on Observability

To determine the effects of various measurement locations, we change the measurement cell from the lower altitudes to the higher altitudes with three measurement quantities, that is, the logarithm $\log(N_e)$ of the number density of electrons, the vertical ion velocity $\mathbf{v}_{ion,vert}$, and the ion temperature T_{ion}.

The problem objective is to estimate $\log(N_e)$, $\mathbf{v}_{ion,vert}$, and T_{ion} in all 50 cells using measurements of $\log(N_e)$, $\mathbf{v}_{ion,vert}$, and T_{ion} in either of the cells 10,20,29, or 40. We assess the observability of each case by comparing the time-averaged rms estimation errors.

In Figure 2(a) shows the spatial distribution of the rms errors with respect to various measurement locations. The overall errors are the smallest for measurements taken in cell 29.

B. Effect of Measurement Quantities on Observability

We now consider all 7 combinations of the available measurement quantities $\log(N_e)$, $\mathbf{v}_{ion,vert}$, and T_{ion} while fixing the measurement location at cell 29. We can thus assess the contribution of each measurement or combination of measurements to estimation accuracy.

Figure 2(b) is the spatial distribution of the rms errors for various combinations of the measurements, and it shows that the measurements of the vertical component of the ion velocity $\mathbf{v}_{ion,vert}$ have a negligible effect on the data assimilation accuracy. Therefore, we can exclude $\mathbf{v}_{ion,vert}$ from measurements for data assimilation without a noticeable loss of accuracy. The cases of $N_e, \mathbf{v}_{ion,vert}$ and $\mathbf{v}_{ion,vert}, T_{ion}$ are similar to the the cases of N_e measurement and T_{ion} measurement, respectively.
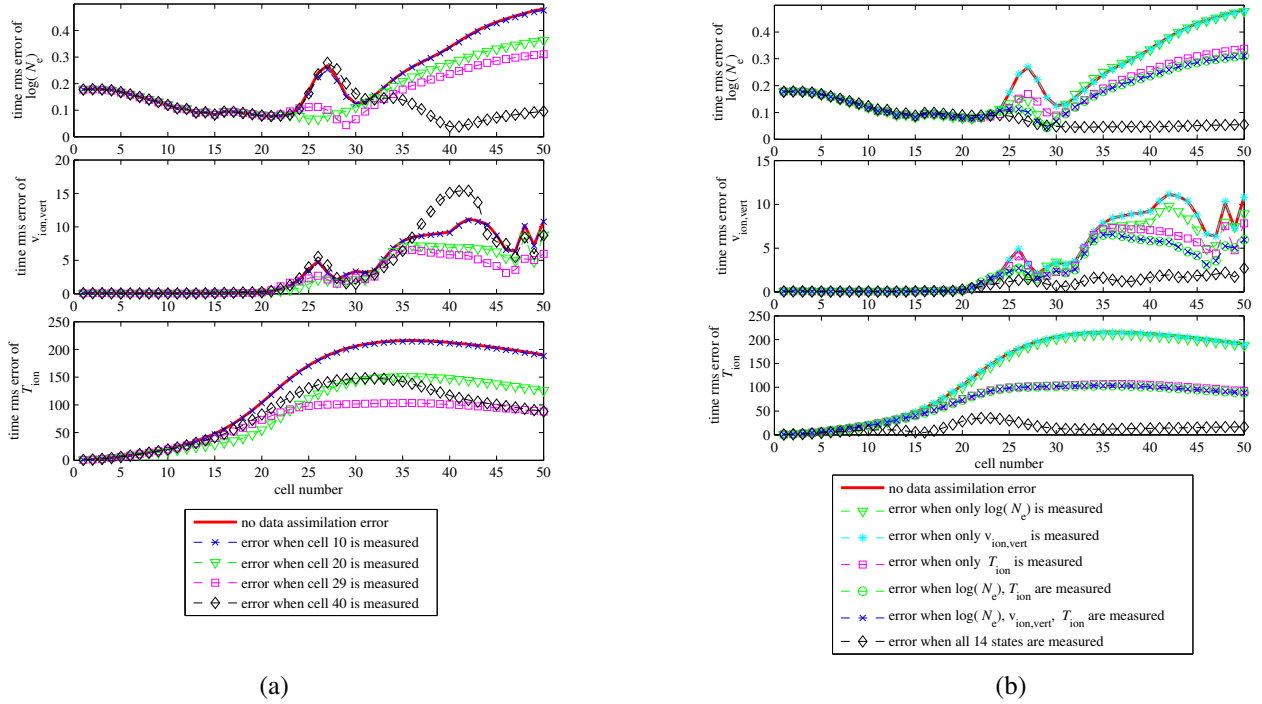
(a)

(b)

Fig. 2. (a) Cell number versus rms errors using measurements from different locations. (b) Cell number versus rms errors using different combination of measurement quantities.
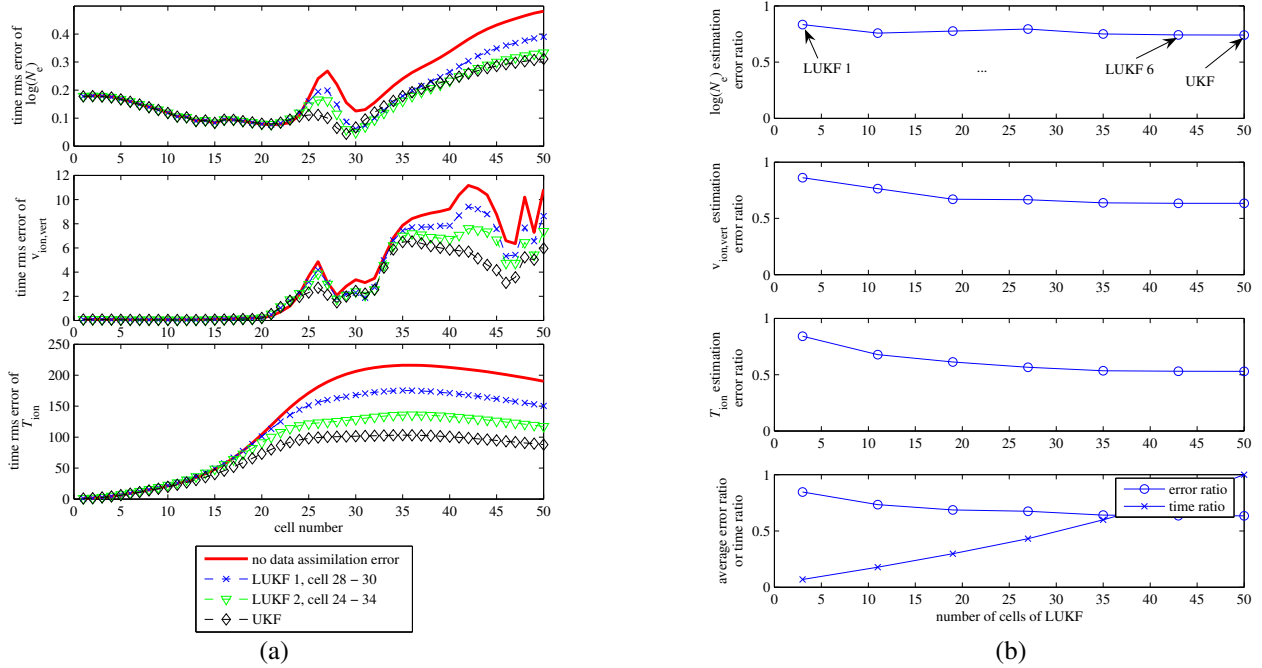

(a)

(b)

Fig. 3. (a) Cell number versus rms errors. (b) Ratio of sum of data assimilation rms errors to the sum of no-data-assimilation errors. The LUKF performance for regions of various sizes are compared with the performance of UKF. All cases use measurements of log number density of electron and ion temperature of cell 29. Spatial regions of LUKF's are, LUKF 1 : cell 28 - 30 (3 cells), LUKF 2 : cell 24 - 34 (11 cells), LUKF 3 : cell 24 - 42 (19 cells), LUKF 4 : cell 24 - 50 (27 cells), LUKF 5 : cell 16 - 50 (35 cells), LUKF 6 : cell 8 - 50(43 cells), Full UKF : cell 1 - 50 (50 cells).

Finally, we perform data assimilation using all 14 states in cell 29, which provides the best accuracy at all altitudes.

VII. LUKF Performance

From the previous section, it is shown that the measurements of N_e, T_{ion} in cell 29 are effective for data assimilation. Therefore, it is expected that we can obtain

the most effective LUKF performance when we choose the LUKF region to include cell 29 and use measurements from cell 29.

Figure 3 compares the UKF and LUKF for localized region of various sizes. The estimation error decreases while the size of the LUKF region increases. Figure 3(b) shows

that the errors of LUKF with the number of cells greater than 11 do not change appreciably, whereas the computation time increases rapidly.

The accuracy of the LUKF estimators with the lower number of LUKF cells is quite close to the accuracy of UKF because of the highly coupled upper cells of vertical 1D GITM. In other words, the ionosphere-thermosphere is highly observable at higher altitudes. Consequently, LUKF can be effectively applied to this kind of example.

VIII. CONCLUSION

We used a localized, sampled-data update scheme with frozen-intersample error covariance to reduce the computational complexity of the vertical 1D GITM data assimilation based on the unscented Kalman filter. We performed the numerical studies to obtain effective measurement locations and quantities for the sampled-data UKF, and then applied the sampled-data LUKF. The sampled-data LUKF with a small local region showed good estimation accuracy in much shorter computation time for data assimilation on the highly coupled vertical 1D GITM.

REFERENCES

[1] C. H. Bishop and Z. Toth, "Ensemble transformation and adaptive observations," *Monthly Weather Rev.*, 56:pp. 1748–1765, 1999.

[2] T. M. Hamill and C. Snyder, "Using improved background-error covariances from an ensemble Kalman filter for adaptive observations," *Monthly Weather Rev.*, 130:pp. 1552–1572, 2002.

[3] S. J. Majumdar, C. H. Bishop, R. Buizza, and R. Gelaro, "A comparison of ensemble transform Kalman filter targeting guidance with ECMWF and NRL total-energy singular vector guidance," *Quart. J. Roy. Meteor. Soc.*, 128:pp. 2527–2549, 2002.

[4] C. H. Bishop, B. Etherton, and S. J. Majumdar, "Adaptive sampling with the ensemble transform Kalman filter, part 1: Theoretical aspects," *Monthly Weather Rev.*, 129:pp. 420–436, 2001.

[5] S. Gillijns, O. Barrero Mendoza, J. Chandrasekar, B. De Moor, D. S. Bernstein, and A. Ridley, "What Is the Ensemble Kalman Filter and How Well Does it Work?," In *Proc. Amer. Contr. Conf.*, pages 4448–4453, Minneapolis, MN, June 2006.

[6] G. Evensen, "Advanced Data Assimilation for Strongly Nonlinear Dynamics," *Monthly Weather Rev.*, 125:pp. 1342–1354, 1997.

[7] A. Doucet, N. de Freitas, and N. J. Gordon, "Sequential Monte Carlo Methods in Practice," Springer, New York, 2001.

[8] B. Ristic, S. Arulampalam, and N. Gordon, "Beyond the Kalman Filter, particle filters for tracking applications," Artech House, Boston, 2004.

[9] S. J. Julier and J. K. Uhlmann, "Unscented Filtering and Nonlinear Estimation," *Proc. of the IEEE*, 92(3):pp. 401–422, March 2004.

[10] S. Thrun, W. Burgard, and D. Fox, "Probabilistic Robotics," The MIT Press, Cambridge, MA, 2005.

[11] J. Chandrasekar, A. Ridley, and D. S. Bernstein, "A Comparison of the Extended and Unscented Kalman Filters for Discrete-Time Systems with Nondifferentiable Dynamics," *Proc. Amer. Contr. Conf*, pp. 4431–4436, New York, NY, July 2007.

[12] J. Chandrasekar, A. J. Ridley, and D. S. Bernstein, "An SDRE-Based Asymptotic Observer for Nonlinear Discrete-Time Systems," *Proc. Amer. Contr. Conf.*, pp. 3630–3635, Portland, OR, June 2005.

[13] J. Chandrasekar, I. S. Kim, and A. J. Ridley, and D. S. Bernstein, "Reduced-Order Covariance-Based Unscented Kalman Filtering with Complementary Steady-State Correlation," *Proc. Amer. Contr. Conf.*, pp. 4452–4457, New York, NY, July 2007.

[14] I. S. Kim, J. Chandrasekar, and H. J. Palanthandalam-Madapusi, A. J. Ridley, and D. S. Bernstein, "State Estimation for Large-Scale Systems Based on Reduced-Order Error-Covariance Propagation," *Proc. Amer. Contr. Conf.*, pp. 5700–5705, New York, NY, July 2007.

[15] D. P. Dee, "On-line Estimation of Error Covariance Paramaters for Atmospheric Data Assimilation," *Monthly Weather Rev.*, 123:pp. 1128–1145, 1995.

[16] T. Penduff, P. Brasseur, C. E. Testut, B. Barnier, and J. Verron, "A four-year eddy-permitting assimilation of sea-surface temperature and altimetric data in the South Atlantic Ocean", *J. of Marine Res.*, 60:pp. 805–833, 2002.

[17] C. E. Testut, P. Brasseur, J. M. Brankart, and J. Verron, "Assimilation of sea-surface temperature and altimetric observations during 1992-1993 into an eddy permitting primitive equation model of the North Atlantic Ocean," *J. of Marine Syst.*, 40-41:pp. 291–316, 2003.

[18] A. J. Ridley, Y. Deng, and G. Toth. "The global ionosphere thermosphere model," *Journal of Atmospheric and Solar-Terrestrial Physics*, 68:pp. 839–864, 2006.

[19] K. Suvanto, "Analysis of incoherent scatter radar data from nonthermal F-region plasma," *Journal of Atmospheric and Terrestrial Physics*, 51(6):pp. 483-495, 1989.

[20] J. L. Anderson, S. L. Anderson, "A Monte Carlo Implementation of the Nonlinear Filtering Problem to Produce Ensemble Assimilation and Forecasts," *Monthly Weather Rev.*, 127: pp.2741–2758, 1999.

[21] J. M. Brankart, C. E. Testut, P. Brasseur, and J. Verron, "Implementation of a multivariate data assimilation scheme for isopycnic ocean models: Application to a 1993-1996 hindcast of the North Atlantic Ocean circulation," *J. Geophys. Res.*, 108(C3):pp. 1–20, 2003.

[22] J. Verron, L. Gourdeau, D. T. Pham, R. Murtugudde, and A. Busalacchi, "An extended Kalman filter to assimilate satellite altimeter data into a nonlinear numerical model of the tropical Pacific: Method and validation," *J. Geophys. Res.*, 104:pp. 5441–5458, 1999.

[23] N. Balan, G. J. Bailey, B. Jenkins, P. B. Rao, R. J. Moffett, "Variation of ionospheric ionization and related solar fluxes during an intense solar cycle," *J. Geophys. Res.* 99(A2):pp. 2243–2254, 2004.

[24] J. Leia, L. Liua, W. Wana, S. Zhangc, "Modeling the behavior of ionosphere above Millstone Hill during the September 21.27, 1998 storm," *J. of Atmospheric and Solar-Terrestrial Physics* 66:pp. 1093–1102, 2004